


# Efficient and Broadband Four-Wave Mixing in a Compact Silicon Subwavelength Nanohole Waveguide

Yuxing Yang, Lu Sun, Yong Zhang, and Yikai Su\*

Confining light in a small volume offers an effective approach to enhance the four-wave mixing (FWM) process. Recently, most efforts are devoted to improve the conversion efficiencies by using resonant structures. As a result, the bandwidths of the FWM conversions are typically limited to 1–2 nm. In this paper, a nonresonant silicon subwavelength nanohole waveguide is proposed to manipulate the field distribution of the propagating wave. The electromagnetic field of the Bloch mode can be engineered to concentrate in the silicon area where the FWM process occurs. Benefiting from the enhanced light intensity, an efficient and broadband FWM process is experimentally demonstrated. A conversion efficiency of  $-26.7$  dB is achieved with a carefully designed silicon nanohole waveguide, showing a 12.5 dB improvement relative to a conventional silicon strip waveguide. The 3 dB conversion bandwidth of the silicon nanohole waveguide is  $\approx 37$  nm, limited by the optical amplifiers employed in the experiment.

Nonlinear optical processes in silicon-based devices have attracted significant attention in recent years, owing to the high index contrasts of silicon-on-insulator (SOI) waveguides that allow tight confinement of the propagating lights.<sup>[1–3]</sup> Four-wave mixing (FWM) is an important third-order Kerr nonlinear effect in silicon for all-optical signal processing functions.<sup>[4–6]</sup> Various silicon photonic devices including microrings,<sup>[7–9]</sup> photonic crystals,<sup>[10–12]</sup> and 1D periodic photonic structures<sup>[13,14]</sup> have been employed to improve the FWM conversion efficiencies by enhancing the light–matter interactions using the resonant structures.<sup>[15–19]</sup> Although a resonant structure can significantly improve the conversion efficiency, the conversion bandwidth is inevitably limited by the cavity bandwidth or the band edge of a photonic crystal. For example, the FWM conversion bandwidth in a photonic crystal waveguide is typically limited to 1–2 nm due to the strong dispersion of the slow light. By engineering the dispersion, a maximum conversion bandwidth of 15 nm was achieved.<sup>[20]</sup> To date, it is still challenging to realize an efficient and broadband FWM process with a low pump power in a compact on-chip silicon device.

Dr. Y. Yang, Dr. L. Sun, Prof. Y. Zhang, Prof. Y. Su  
State Key Lab of Advanced Optical Communication Systems and Networks  
Department of Electronic Engineering  
Shanghai Jiao Tong University  
Shanghai 200240, China  
E-mail: yikaisu@sjtu.edu.cn

 The ORCID identification number(s) for the author(s) of this article can be found under <https://doi.org/10.1002/adom.201900810>.

DOI: 10.1002/adom.201900810

In this paper, we propose a simple yet effective scheme by using a compact silicon subwavelength nanohole waveguide, which possesses a broadband and low-loss transmission. As the subwavelength nanoholes are periodically distributed along the silicon waveguide, the optical properties of this artificial material, such as the effective refraction index, the transmittance and the dispersion, can be engineered by varying the nanohole diameter and the period. By this means, an enhanced light intensity in the silicon area can be achieved in the nanohole waveguide, leading to an efficient and broadband FWM process. The mechanism we propose in this paper is different from the slow-wave effect reported in previous papers,<sup>[13,14]</sup> which enhanced the conversion efficiencies in 1D periodic photonic structures by lever-

aging the large group indices near the band edges. The nonlinearity of the silicon nanohole waveguide originates from the enhanced light intensity in the nonresonant silicon waveguide, thus enabling a broadband FWM process. For the nanoholes with a diameter of 100 nm and a period of 300 nm, a FWM conversion efficiency of  $-26.7$  dB is observed in the experiment, showing a 12.5 dB improvement compared to a conventional silicon strip waveguide. Thanks to the broadband transmission and the negligible linear dispersion of the silicon nanohole waveguide, a 3 dB conversion bandwidth of 37 nm is experimentally demonstrated, which is limited by the optical amplifiers employed in the experiment.

The proposed silicon nanohole waveguide is schematically illustrated in **Figure 1a**, which consists of a periodic array of subwavelength nanoholes in the center of the silicon waveguide. The propagation of the light in the waveguide is studied using the 3D finite-difference time-domain (3D-FDTD) method. In **Figure 1b–d**, the cross-section of the silicon waveguide is  $480 \times 220$  nm<sup>2</sup> and the lengths of the silicon waveguide and the nanohole segment are 60 and 50  $\mu$ m, respectively. The nanohole diameter  $d = 100$  nm is used and kept constant while the period of the nanoholes is varied. The electric field distribution of the Bloch mode is mainly trapped in the air (silicon) area with the period  $a = 200$  nm ( $a = 300$  nm). Based on the previous study,<sup>[21]</sup> the band edge wavelength is dependent on the nanohole period. The normalized transmission spectra with two periods and different nanohole diameters are shown in **Figure 1e,f**, respectively. It can be seen that the band edges in both cases are away from the operating wavelengths (C-band) with the nanohole diameters ranging from 60 to 140 nm. Small

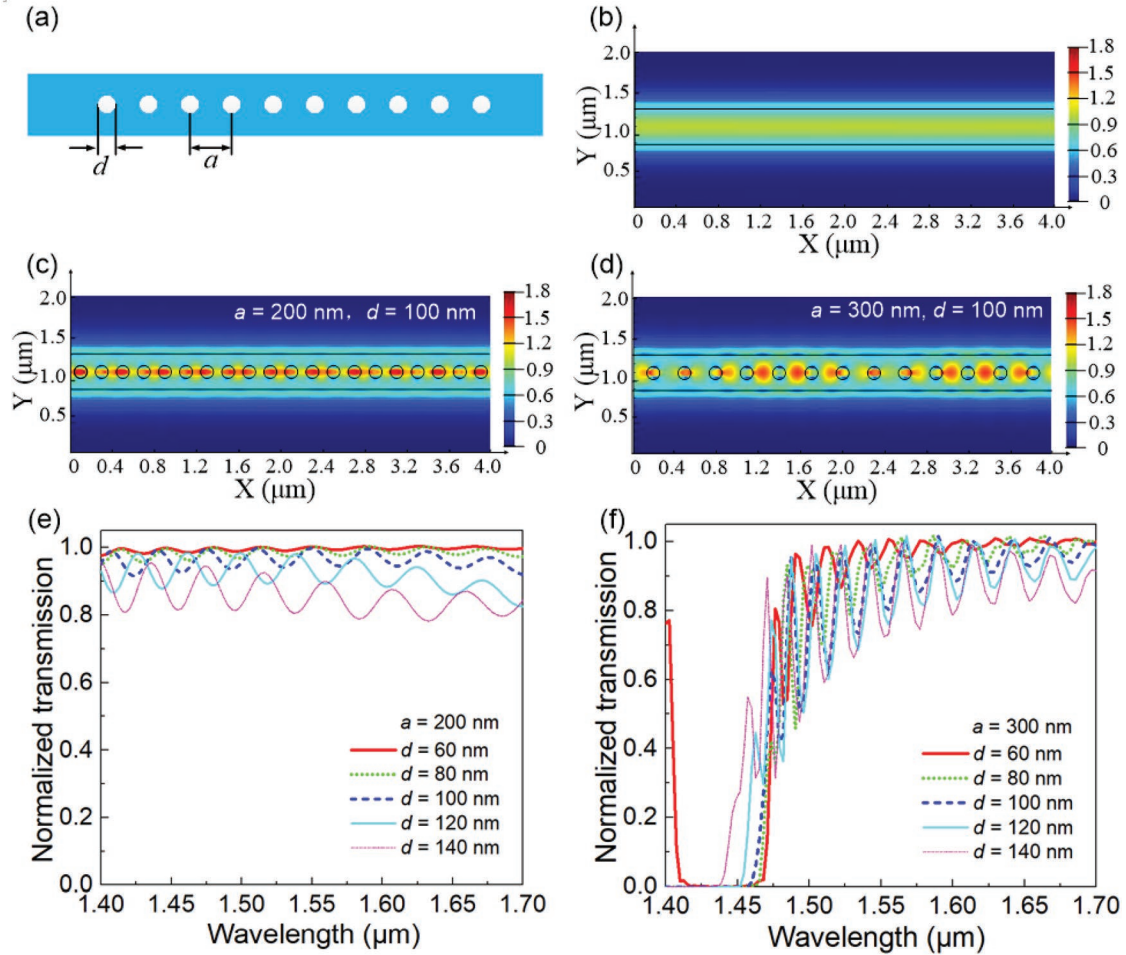


**Figure 1.** a) Schematic diagram of the silicon nanohole waveguide. b–d) Simulated electric field distribution in the silicon strip waveguide (b) and the nanohole waveguides with c)  $a = 200$  nm and d)  $a = 300$  nm, respectively, where  $d = 100$  nm and  $\lambda = 1550$  nm. e, f) Normalized transmission spectra of the silicon nanohole waveguides with e)  $a = 200$  nm and f)  $a = 300$  nm.

ripples appear in the transmission spectra due to the minor reflections at the interfaces between the strip waveguide and the nanohole segment. The ripples become stronger with larger nanohole diameters and at wavelengths near the band edge. Therefore, the electric field distribution and the transmission loss of the silicon nanohole waveguide can be engineered by tuning the nanohole diameter and the period. If  $a = 300$  nm, the electromagnetic field of the Bloch mode is nonuniform and more concentrated in the silicon section compared to the silicon strip waveguide (Figure 1b). As a result, an enhanced nonlinearity can be obtained in the silicon nanohole waveguide. Considering the transmission loss and the fabrication limitations, the nanohole diameter of 100 nm and the period of 300 nm are used in our experiment.

To study the origin of the high nonlinearity in the proposed device, we calculate the conversion efficiency  $G_{\text{idler}}$  of the degenerate FWM process in the waveguide, which is given by<sup>[4,22]</sup>

$$G_{\text{idler}} = P_{\text{idler}}^{\text{out}} / P_{\text{signal}}^{\text{in}} = (\gamma P_{\text{pump}} \sinh(gL)/g)^2 \quad (1)$$

$$g = \left[ \gamma P_{\text{pump}} \Delta k_{\text{linear}} - (\Delta k_{\text{linear}}/2)^2 \right]^{1/2} \quad (2)$$

$$\Delta k_{\text{linear}} = -\beta_2 (\Delta\omega)^2 - \frac{1}{12} \beta_4 (\Delta\omega)^4 \quad (3)$$

$$\gamma = 2\pi n_2 / \lambda A_{\text{eff}} \quad (4)$$

where  $P_{\text{idler}}^{\text{out}}$  and  $P_{\text{signal}}^{\text{in}}$  are the output idler and the input signal powers, respectively,  $\gamma$  is the effective nonlinearity,  $P_{\text{pump}}$  is the pump power,  $g$  is the parametric gain parameter,  $L$  is the interaction length,  $\Delta k_{\text{linear}}$  is the linear phase-mismatch,  $\beta_2$  and  $\beta_4$  are the second- and fourth-order dispersion parameters at the pump wavelength,  $\Delta\omega$  is the frequency difference between the pump and signal lights,  $n_2$  is the nonlinear refractive index,  $\lambda$  is the wavelength of light, and  $A_{\text{eff}}$  is the effective mode area. Equation (1) shows the conversion efficiency of the FWM process in the non-resonant structure and neglects the effects of pump depletion. For the linear phase-mismatch  $\Delta k_{\text{linear}}$ , only the even-order dispersion terms play a role due to the symmetry of the FWM process.<sup>[22]</sup> In Equation (3), only the dispersion effects up to the fourth-order are taken into account. Note that the effective mode area varies as the cross section changes along the waveguide, so the effective nonlinearity also depends on the propagation length in our case.

Figure 2a,b shows the group index, the second- and fourth-order dispersion parameters of the silicon nanohole waveguide

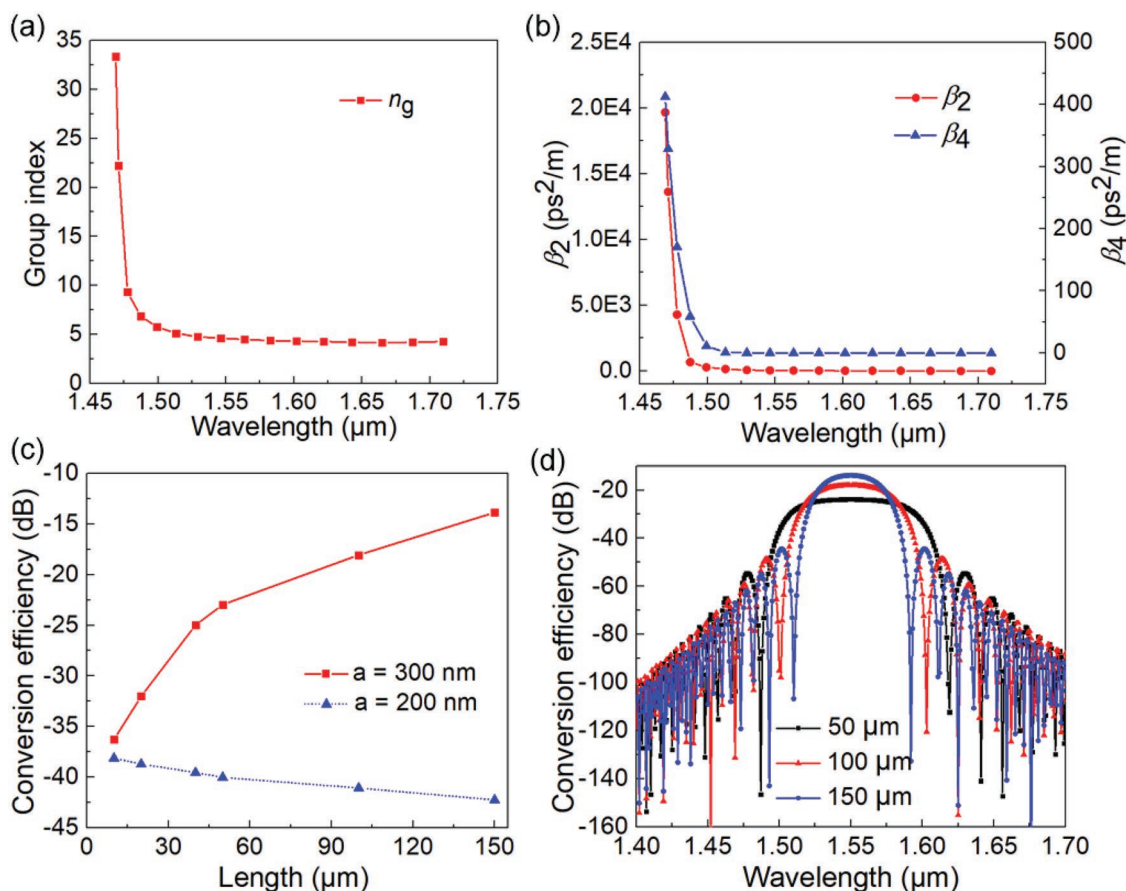


**Figure 2.** a) Simulated group index of the silicon nanohole waveguide with  $d = 100$  nm and  $a = 300$  nm. b) Second- (red solid curve with circles) and fourth-order (blue solid curve with triangles) dispersion parameters of the silicon nanohole waveguide. c) Simulated conversion efficiency as a function of the length of the nanohole segment. d) Simulated conversion bandwidths of the silicon nanohole waveguides with different nanohole-segment lengths.

derived from the 3D-FDTD simulations. For the silicon nanohole waveguide with  $d = 100$  nm and  $a = 300$  nm, the group index ( $n_g$ ), the second- ( $\beta_2$ ) and fourth-order ( $\beta_4$ ) dispersion parameters increase rapidly as the wavelength gets close to 1460 nm where the band edge locates. At the wavelength of 1550 nm, the group index of the silicon nanohole waveguide is 4.53, indicating that the slow-wave effect is minor in our case. The FWM process in the silicon nanohole waveguide was also numerically studied using the 3D-FDTD method, and the conversion efficiency is shown in Figure 2c as a function of the length of the nanohole segment. For the nanohole waveguide with  $a = 300$  nm, the conversion efficiency increases from  $-36.2$  to  $-13.8$  dB as the length varies from 10 to 150  $\mu\text{m}$ . As a comparison, the conversion efficiency in a 3 mm long silicon strip waveguide without nanoholes is  $-38.2$  dB under the same pump power of 100 mW. It proves that the silicon nanohole waveguide can significantly enhance the nonlinearity with the strongly confined light, in the absence of the slow-wave effect. It should be noted that the absorption losses including the material absorption, two-photon absorption, and free-carrier absorption are not considered in the simulations. The conversion efficiency increases with nanohole length until significant phase-mismatching occurs at longer propagation lengths.

In the experiment, due to the device loss and the absorption loss, the conversion efficiency is limited to a  $-25$  dB level if the nanohole segment length exceeds 50  $\mu\text{m}$ . For the nanohole waveguide with  $a = 200$  nm, the conversion efficiency decreases slowly with the increase of the nanohole segment length. This is because the nanohole segment contributes less to the conversion efficiency, and the conversion efficiency is mostly determined by the silicon strip waveguide in this case. Figure 2d presents the theoretical FWM conversion bandwidths calculated by Equation (1). If the nanohole-segment length changes from 50 to 150  $\mu\text{m}$ , the conversion efficiency becomes higher, while the conversion bandwidth reduces. For the case of 50  $\mu\text{m}$  long nanohole segment length, the second- and fourth-order dispersion parameters are nearly zero at wavelengths close to 1550 nm, so the linear phase-mismatching can be neglected compared with the nonlinear phase-mismatching ( $\Delta k_{\text{nonlinear}} = 2\gamma P_{\text{pump}}$ ). As a result, a 3 dB conversion bandwidth of  $\approx 80$  nm is obtained in theory.

The silicon nanohole waveguide was fabricated on a silicon-on-insulator wafer with a 220 nm thick top silicon layer. In order to increase the butt-coupling efficiency between the tapered-lens fibers and the silicon waveguide, two silicon inverse tapers and a thick silica cover layers were employed.

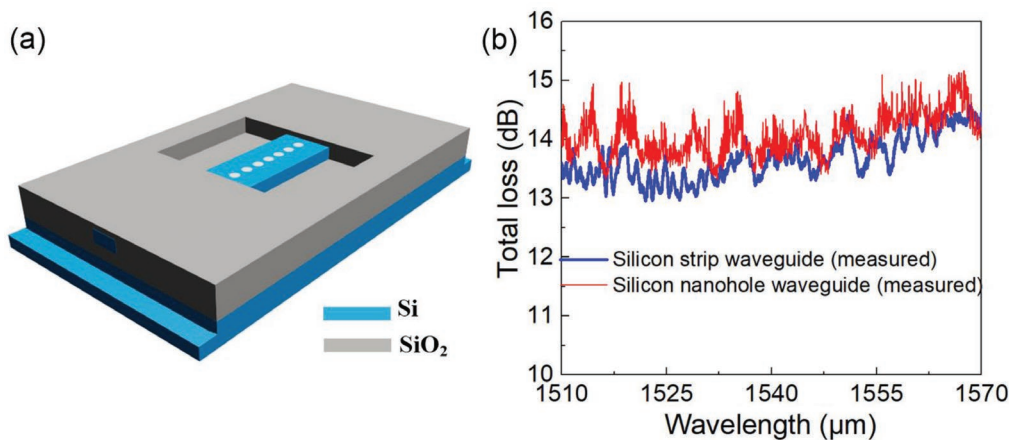


**Figure 3.** a) 3D view of the fabricated silicon nanohole waveguide. b) Measured total losses of the silicon nanohole waveguide (red solid curve) and the strip waveguide (blue solid curve), respectively.

To obtain high index contrast and tight light confinement, the nanoholes in the center of the silicon waveguide should not be covered with the silica top layer. Thus, a windowed silica layer on the silicon waveguide was designed, and the fabrication processes were the same as previously described in our work.<sup>[23]</sup>

The 3D view of the fabricated silicon nanohole waveguide is depicted in **Figure 3a**. The device was fabricated by etching periodic nanoholes in the silicon strip waveguide. The silicon strip waveguide has a 3 mm total length and a  $480 \text{ nm} \times 220 \text{ nm}$  cross-section. The diameter, period, and length of the nanohole segment are 100, 300, and  $50 \mu\text{m}$  respectively. The length of the silica window is longer than that of the nanohole segment. **Figure 3b** plots the measured total losses of the silicon strip waveguide and the nanohole waveguide, respectively, including the coupling losses. As can be seen, the total losses of the silicon strip waveguide and the nanohole waveguide are almost independent of the wavelength in the range of 1510–1570 nm. In the experiment, the coupling loss between the tapered-lens fiber and the silicon waveguide is  $\approx 6.5 \text{ dB}$  per facet, which can be further reduced by increasing the thickness of the up-cladding silica layer.

The degenerate FWM experiment was performed using the setup shown in **Figure 4**. A continuous-wave (CW) light at a wavelength of 1550.07 nm was amplified by an erbium-doped fiber amplifier (EDFA, KEOPSYS CEFA-C-PB-HP), serving as the pump light. A tunable CW laser was amplified

with another EDFA and used as the signal light source. The amplified spontaneous emissions were respectively filtered by a pair of filters. The polarization controllers (PCs) were applied to ensure that the input light is TE-polarized. The pump and the signal lights were combined in a 50:50 coupler and coupled into the device under test (DUT) through a tapered-lens fiber with a  $2 \mu\text{m}$  diameter tip. The output spectra were measured with the optical spectrum analyzer (OSA, Yokogawa, AQ6370C). An isolator and a variable optical attenuator (VOA) were employed to prevent the damage caused by the reflected light from the device and the high output power into the OSA, respectively. The inset shows the scanning electron microscope (SEM) image of the silicon nanohole waveguide under test with  $d = 100 \text{ nm}$  and  $a = 300 \text{ nm}$ .

The output spectra from the silicon strip waveguide and the nanohole waveguide are compared in **Figure 5a**. The length of the nanohole segment was  $50 \mu\text{m}$ , and the total lengths of the both devices were 3 mm. After coupled into the device, the pump and signal powers were set to be 19.7 dBm at 1550.07 nm and 8.7 dBm at 1549.26 nm, respectively. The idler power of the silicon nanohole waveguide was  $-29.5 \text{ dBm}$ , with a 6.5 dB output coupling loss and a 5 dB VOA attenuation. Here, the FWM conversion efficiency is defined as the ratio of the output idler power to the input signal power.<sup>[4]</sup> Thus, the conversion efficiency of the silicon nanohole waveguide was  $-26.7 \text{ dB}$ , improved by 12.5 dB with respect to the strip waveguide. **Figure 5b** shows the relationship between the conversion

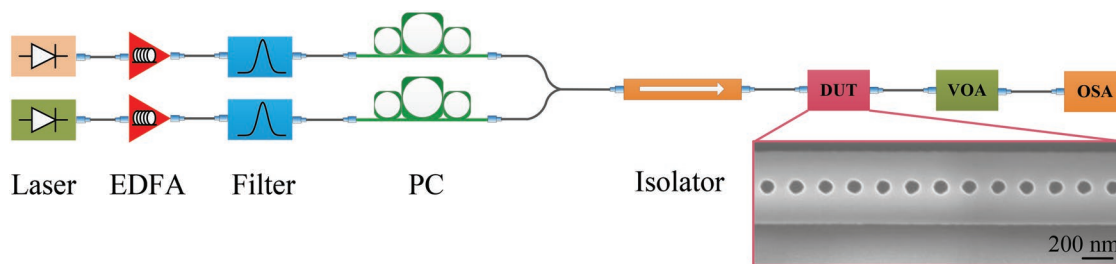


**Figure 4.** Experimental setup for testing the degenerate FWM in the fabricated device. Inset shows the SEM image of the fabricated silicon nanohole waveguide with  $d = 100 \text{ nm}$  and  $a = 300 \text{ nm}$ .



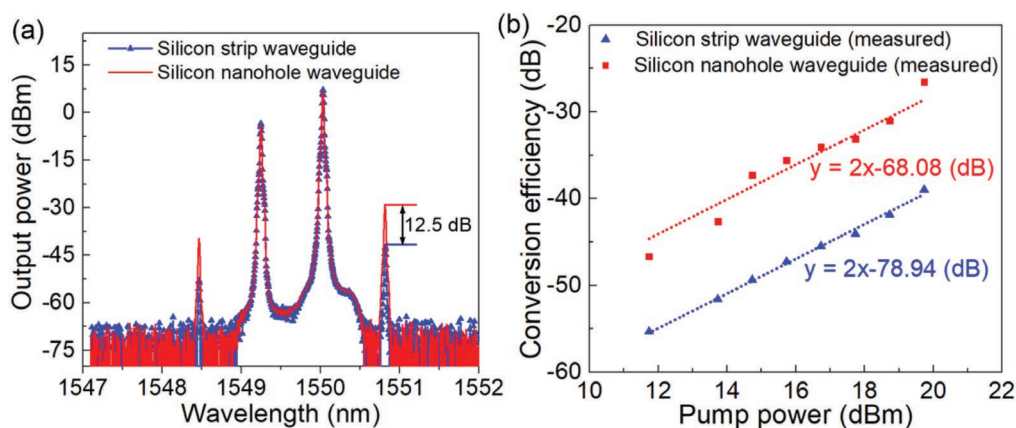


**Figure 5.** a) Measured output spectra of the silicon strip waveguide (blue solid curve with triangles) and the silicon nanohole waveguide (red solid curve). b) Measured conversion efficiencies of the silicon waveguide (blue triangles) and the silicon nanohole waveguide (red squares) as functions of the input pump power.

efficiency and the pump power launched into the devices. If the pump power was increased from 11.7 to 19.7 dBm, the conversion efficiency increased linearly with the pump power. The slopes of 2 were derived from the fitting curves, indicating that the idler power was produced by the FWM process and the nonlinear losses were not significant in our devices.<sup>[24]</sup> From the fitting curve, the average conversion efficiency of the silicon nanohole waveguide is improved  $10.9 \pm 1.6$  dB compared with a conventional silicon strip waveguide at the maximum pump power. As a result, the conversion efficiency can be enhanced by further increasing the pump power, while the maximum pump power is limited to 19.7 dBm by the EDFA employed in our experiment.

The 3 dB conversion bandwidth of the silicon nanohole waveguide was measured and displayed in **Figure 6a**. In the experiment, the pump and the signal powers were set to 19.7 and 8.7 dBm, respectively. According to Equation (2), the conversion bandwidth is related to the effective nonlinearity  $\gamma$ , the input pump power  $P_{\text{pump}}$ , and the linear phase mismatch

$\Delta k_{\text{linear}}$ . As discussed previously, the linear phase mismatch can be neglected compared to the large effective nonlinearity and the high input pump power. The signal wavelength was varied from 1529.26 to 1566.26 nm while the pump wavelength was fixed at 1550.07 nm, showing an operation bandwidth of 37 nm, which is limited by the bandwidth of the EDFA. The measured output spectra are shown in **Figure 6b** with the signal wavelengths located at Point A and Point B indicated in **Figure 6a**, respectively.

In **Figure 7**, the conversion efficiency is measured as a function of the length of the nanohole segment. For the silicon strip waveguide without nanoholes, the conversion efficiency is  $-39.2$  dB. As the length of the nanohole segment increases from 20 to 50  $\mu\text{m}$ , the conversion efficiency of the silicon nanohole waveguide is enhanced significantly, which is in reasonable agreement with the numerical simulation results. However, if the length of the nanohole segment increases to beyond 50  $\mu\text{m}$ , the conversion efficiency is limited to the  $-25$  dB level by the two-photon absorption

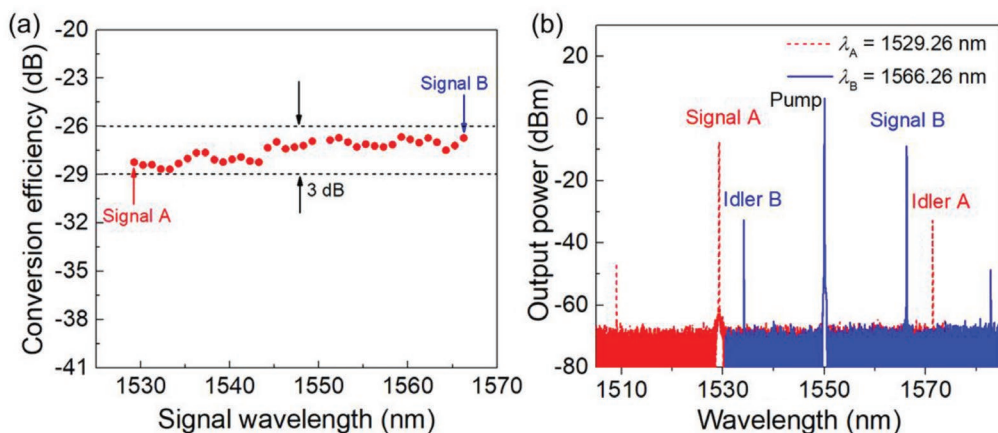


**Figure 6.** a) Conversion efficiency of the silicon nanohole waveguide as a function of the signal wavelength when the pump wavelength is 1550.07 nm. b) Measured output spectra from the silicon nanohole waveguide with the signal wavelengths marked by A and B in a), respectively.  $\lambda_A = 1529.26$  nm (red dashed curve) and  $\lambda_B = 1566.26$  nm (blue solid curve).

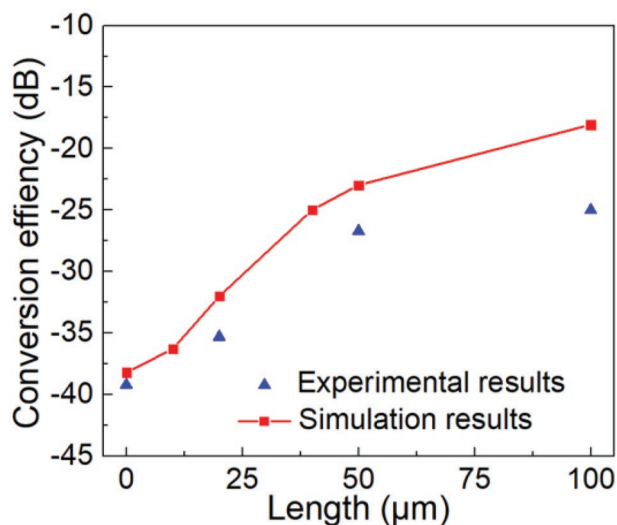


**Figure 7.** Measured and simulated conversion efficiencies of the silicon nanohole waveguide as a function of the length of the nanohole segment.

and the free-carrier absorption effects in silicon, which can be mitigated by reducing the free-carrier lifetime through a reverse biased PIN diode as an example.<sup>[7]</sup>

In summary, we proposed a nonresonant silicon subwavelength nanohole waveguide. By properly designing the diameter and the period of the nanoholes, the light can be tightly confined in the silicon section, leading to a great enhancement of the electric field intensity. Benefitting from the high field concentration, we theoretically and experimentally demonstrated an efficient and broadband FWM process. The FWM conversion efficiency of the silicon subwavelength nanohole waveguide can be as high as  $-26.7$  dB with a  $50$   $\mu\text{m}$  nanohole segment length, showing a  $12.5$  dB improvement relative to the silicon strip waveguide. In addition, owing to the nonresonant structure and the negligible linear dispersion of the silicon nanohole waveguide, a  $3$  dB conversion bandwidth of  $37$  nm is achieved. These interesting results indicate that the silicon nanohole waveguide could be a simple yet effective artificial material to build nonlinear silicon photonic devices for all-optical signal processing.

## Acknowledgements

The work was supported in part from the National Key R&D Program of China under grant 2016YFB0402501 and the National Natural Science Foundation of China (NSFC) (61835008, 61605112). The authors thank the Center for Advanced Electronic Materials and Devices (AEMD) of Shanghai Jiao Tong University (SJTU) for the support in device fabrications.

## Conflict of Interest

The authors declare no conflict of interest.

## Keywords

four-wave mixing, integrated devices, nonlinear optics, optical nanostructures

Received: May 14, 2019

Revised: July 13, 2019

Published online: August 20, 2019

- [1] J. Leuthold, C. Koos, W. Freude, *Nat. Photonics* **2010**, *4*, 535.
- [2] N. A. Gsken, M. P. Nielsen, N. B. Nguyen, S. A. Maier, R. F. Oulton, *Opt. Express* **2018**, *26*, 30634.
- [3] K. Li, A. C. Foster, *Proc. IEEE* **2018**, *106*, 2196.
- [4] M. A. Foster, A. C. Turner, J. E. Sharping, B. S. Schmidt, M. Lipson, A. L. Gaeta, *Nature* **2006**, *441*, 7096.
- [5] Q. Lin, O. J. Painter, G. P. Agrawal, *Opt. Express* **2007**, *15*, 25.
- [6] C. Koos, P. Vorreau, T. Vallaitis, P. Dumon, W. Bogaerts, R. Baets, B. Esembeson, I. Biaggio, T. Michinobu, F. Diederich, W. Freude, J. Leuthold, *Nat. Photonics* **2009**, *3*, 216.
- [7] J. R. Ong, R. Kumar, R. Aguinaldo, S. Mookherjea, *IEEE Photonics Technol. Lett.* **2013**, *25*, 17.
- [8] A. C. Turner, M. A. Foster, A. L. Gaeta, M. Lipson, *Opt. Express* **2008**, *16*, 7.
- [9] M. J. Strain, C. Lacava, L. Meriggi, I. Cristiani, M. Sorel, *Opt. Lett.* **2015**, *40*, 1274.
- [10] M. Ebnali-Heidari, C. Monat, C. Grillet, M. K. Moravvej-Farshi, *Opt. Express* **2009**, *17*, 20.
- [11] J. Li, L. O'Faolain, I. H. Rey, T. F. Krauss, *Opt. Mater. Express* **2011**, *1*, 5.
- [12] M. Lonar, D. Nedeljkovi, T. P. Pearsall, J. Vukovi, A. Scherer, S. Kuchinsky, D. C. Allan, *Appl. Phys. Lett.* **2002**, *80*, 1689.
- [13] D. W. Kim, S. H. Kim, S. H. Lee, H. S. Jong, J.-M. Lee, E.-H. Lee, K. H. Kim, *Opt. Express* **2013**, *21*, 24.
- [14] J. Garcia, P. Sanchis, A. Martınez, J. Martı, *Opt. Express* **2008**, *16*, 5.
- [15] C. Monat, B. Corcoran, M. E.-Heidari, C. Grillet, B. J. Eggleton, T. P. White, L. O'Faolain, T. F. Krauss, *Opt. Express* **2009**, *17*, 2944.
- [16] J. R. Ong, M. L. Cooper, G. Gupta, W. M. J. Green, S. Assefa, F. Xia, S. Mookherjea, *Opt. Lett.* **2011**, *36*, 2964.
- [17] S. Azzini, D. Grassani, M. Galli, D. Gerace, M. Patrini, M. Liscidini, P. Velha, D. Bajoni, *Appl. Phys. Lett.* **2013**, *103*, 031117.
- [18] C. Monat, M. E.-Heidari, C. Grillet, B. Corcoran, B. J. Eggleton, T. P. White, L. O'Faolain, J. Li, T. F. Krauss, *Opt. Express* **2010**, *18*, 22.
- [19] J. F. McMillan, M. Yu, D.-L. Kwong, C. W. Wong, *Opt. Express* **2010**, *18*, 15484.
- [20] S. A. Schulz, L. O'Faolain, D. M. Beggs, T. P. White, A. Melloni, T. F. Krauss, *J. Opt.* **2010**, *12*, 104004.
- [21] D. Goldring, U. Levy, I. E. Dotan, A. Tsukernik, M. Oksman, I. Rubin, Y. David, D. Mendlovic, *Opt. Express* **2008**, *16*, 5585.
- [22] M. A. Foster, A. C. Turner, R. Salem, M. Lipson, A. L. Gaeta, *Opt. Express* **2007**, *15*, 12949.
- [23] Y. Yang, Z. Xu, X. Jiang, Y. He, X. Guo, Y. Zhang, C. Qiu, Y. Su, *Photonics Res.* **2018**, *6*, A10.
- [24] H. Fukuda, K. Yamada, T. Shoji, M. Takahashi, T. Tsuchizawa, T. Watanabe, J.-i. Takahashi, S.-i. Itabashi, *Opt. Express* **2005**, *13*, 4629.